Characterisation of Mushroom Structures on Airfoils: CFD and Wind Tunnel Investigation

Sarlak Chivaee, Hamid; Sørensen, Jens Nørkær

Link back to DTU Orbit

Characterisation of Mushroom Structures on Airfoils: CFD and Wind Tunnel Investigation

H. Sarlak and J.N. Sørensen

Department of Wind Energy

Technical University of Denmark, 2800 Kgs. Lyngby, Denmark

Abstract

We presents the latest numerical and experimental findings on formation of such 3D flow structures over an NREL S826 airfoil at Reynolds numbers below 200,000. The spanwise flow is first detected by comparing polars measured using both surface pressure integration at one cross section as well as integral force gauge measurement, and the surface oil flow visualization technique is subsequently used to study the 3D flow topologies formed on the airfoil. Numerical simulations of the same setup are also performed using the k-ω SST variant of unsteady Reynolds-Averaged Navier-Stokes (RANS) and the results are validated using wind tunnel experiments. CFD is shown to be able to accurately predict the lift and drag and qualitatively observe stall cells similar to the experiments.

Introduction

Lifting surfaces, such as wings or wind turbine blades, are often designed using two-dimensional airfoil polars assuming little or no mutual influence between the spanwise elements. However, the 2D flow on rectangular wings occasionally produces 3D "mushroom" structures at high angles of attack due to the periodic spanwise breakdown of vortices that are created on the airfoil suction side (see (Ghassemi Isfahani, Webb, & Samimy, 2017; Manolesos & Voutsinas, 2014; Winkelman & Barlow, 1980)). This article presents the latest numerical and experimental findings on formation of such 3D flow structures over an NREL S826 airfoil at Reynolds numbers below 200,000.

Experimental set ups

Oil-flow visualization experiment is performed in a low speed wind tunnel facility a cross section of which is shown in figure 1. The tunnel's test section is 1.3 by 0.5 by 0.5 m in streamwise, lateral, and vertical directions, respectively, and has a contraction ratio of 1:12.5, capable of delivering a uniform maximum velocity of U=65 m/s with a maximum turbulent intensity of about 0.1%. The airfoil used for the visualizations has a chord length of c=0.1m and a span of b=0.5 m giving a span to chord ratio of 5 and there is no gap between the airfoil and the tunnel side walls. The material for flow visualization is a mixture of Titanium dioxide, Talc powder, Linseed oil, Lamp oil, Normal petroleum, and Oleic acid. For further information about the mixture and a more detailed investigation see (Sarlak, Fr re, Mikkelsen, & Sørensen, 2018).
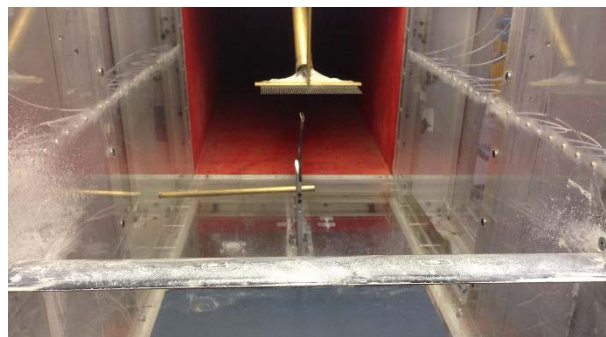

Figure 1. Placement of the horizontally mounted airfoil in the low speed wind tunnel for oil-flow visualisations.

Numerical set ups

Numerical simulations have been performed using a general purpose block structured flow solver, EllipSys3D (Michelsen, 1992; Sørensen, 1995). Governing equations are solved using finite volume discretization of the primitive variables stored in collocated grids. The convective terms are discretized using a third order accurate QUICK scheme. Time is discretized using a second order backward Euler scheme and the solution is marched in time using inner time stepping where the number of each pseudo time step can be either specified or remain as a function of the residuals. Pressure checker boarding is prevented by using Rhie-Chow interpolation on a collocated grid arrangement and the pressure correction equation is solved using PISO algorithm. Following a grid refinement study, a computational c-mesh comprising of 256 by 256 cells around and in the normal direction of the airfoil and 64 cells per span is used for the simulations.
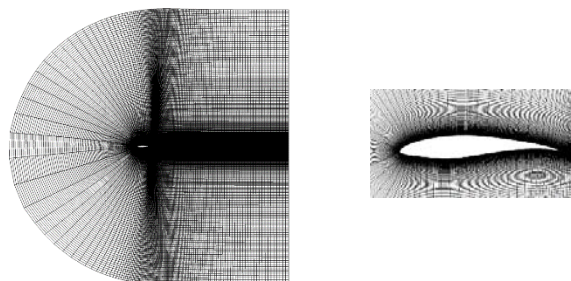

Figure 1: Computational domain and the C-mesh used for the simulations

Results

First, we will present the wake flow structures at Re=100,000 and four different angles of attack at mid-span. The time averaged wake velocity profiles as well as error bars of standard

deviation are also shown (figure 2). Such results can be used for validation of numerical models among other applications.
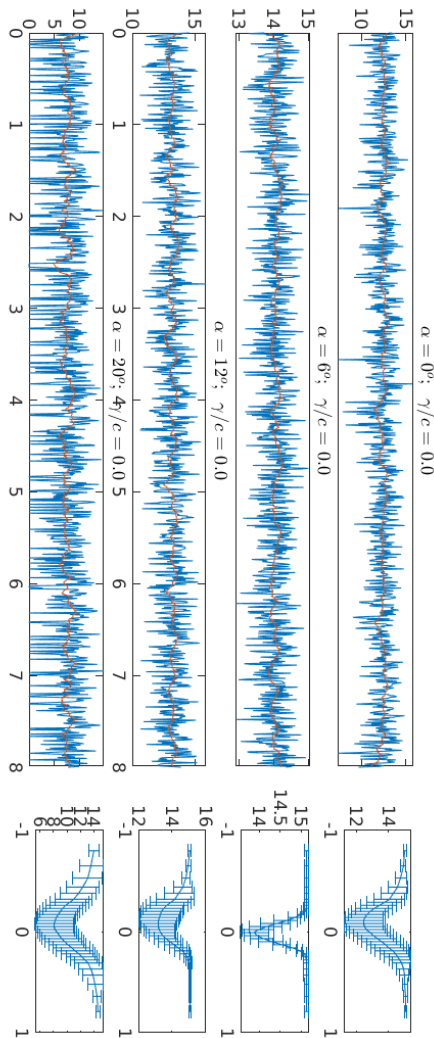

Figure 2: Time history of the wake velocities at Re = 100,000 for different angles of attack (top) and the corresponding time averaged wake velocities (bottom).

Figure 3 shows the wake velocities measured by the wake rake in the upstroke (0-20°) as well as downstroke (20-0°). Normally, the polars as well as wake velocities in each angle of attack are independent of the previous angle therefore the wake plot is assumed to be symmetric around 20°. In figure 2 however, a clear asymmetry can be seen around stall angles of attack as shown by the red markers. This is an indication of the so called stall hysteresis and is typical in certain airfoil types and Reynolds numbers. The reader is referred to Sarlak et al., (2018) for further investigation of the phenomena.
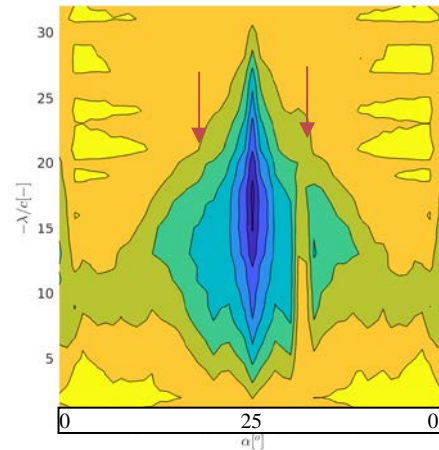

Figure 3. Graphical representation of the wake velocities measured by the wake rake, indicating asymmetry near stall angles in upstroke vs. downstroke pitching

Investigation of 3D flow structures

This section investigates 3-dimensionality of the flow on the airfoil suction side. As the first indication, we have measured the lift using the integral force magnitude (force gauge) – Cl_g, as well as pressure integration over the pressure taps abound a particular airfoil section – Cl_p. Figure 4 shows the difference in both measured magnitudes. As can be seen, there is a significant discrepancy between the measured values suggesting the 3D effects. The 3D effects will now be discussed visually in more detail.
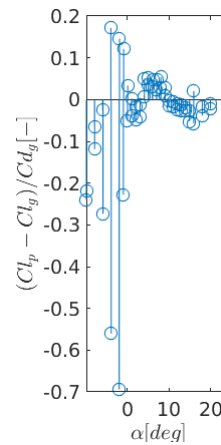

Figure 4: Discrepancies in measurements of lift using surface pressure (Cl_p), and force gauge (Cl_g). High deviation indicates 3D flow effects since Cl_p is only measured at one cross secion whereas Cl_g is an integral value over the whole span.

We next will investigate flow structures formed on the airfoil at various Reynolds numbers and angles of attack. Figure 5 shows the oil flow visualisation results. As can be seen from the Re=40,000 case, a clear shift in separation line towards the leading edge is seen with increasing angle of attack. The trend is, however, not as clear for higher angles of attack. A major observation is that for Re=100,000 and 200,000, at AOA=12° (and to a weaker degree 15°), a clear stall cell pattern is visible. At 20°, flow is fully separated at the leading edge. Finally, flow at AOA=0° and 6° exhibits laminar separation and reattachment in the mid-chord region followed by trailing edge separation.

Figure 5: Oil-flow visualisations at various Reynolds numbers and angles of attack 20º, 15º, 12º, 6º, and 0º from top to bottom.

Finally, we investigate the corner flows in order to arrive at an estimate of the vertical extent of flow separation. As shown in figure 6 and in-line with previous observations, separation location moves towards the leading edge with increasing angle of attack. It is also observed that as the angle of attack increases, a visible vortex is formed on the airfoil corner adjacent to the wall.

Figure 6: Visualisation of flow structures at the wind tunnel walls for Re = 200,000 at different angles of attack.

In the next section, we will numerically investigate formation of stall cells.

CFD validations

Figure 7 shows snapshots of instantaneous streamwise velocity at different angles of attack for Re=100,000. As can bee seen, the flow over most parts of the airfoil remains attached at an angle of attack of 0o. As the angle of attack is increased, the wake behind airfoil becomes wider and trailing edge separation occurs.
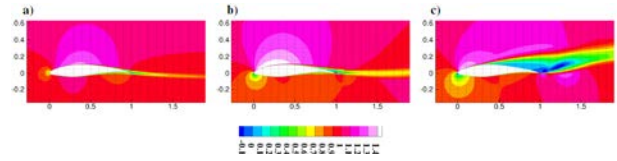

Figure 7. Streamwise velocity contours on the S826 airfoil at Reynolds numbers 100,000 and angles of attack 0º and 6º, respectively.

To quantify the accuracy of CFD simulations, polars are compared against wind tunnel measurements by Sarlak, Mikkelsen, Sarmast, & Sørensen, (2014). As can be seen from figure 8, a very good agreement is seen at all studied angles of attack.
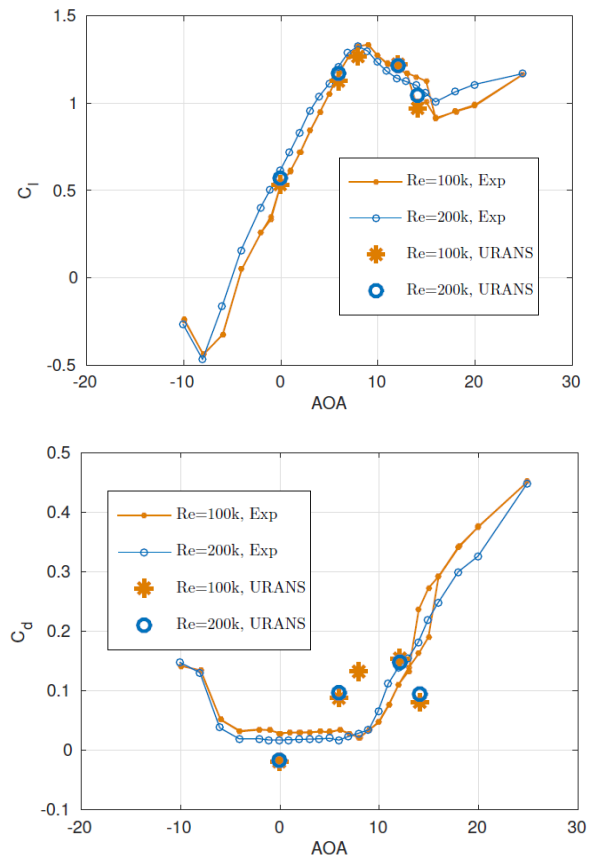

Figure 8: Comparison of time-averaged lift (top) and drag (bottom) coefficients from URANS, for the case of AR=5, with experimental data (Sarlak et al., 2014)

Knowing that the CFD simulations have a good accuracy in terms of predicting the right polars, it is finally desired to study and compare the stall cell predictions by CFD. Figure 9 shows reproduction of the experimental data at Re=100,000 by RANS simulations at angle of attack 12º. As can be seen, a good qualitative agreement is seen between the data
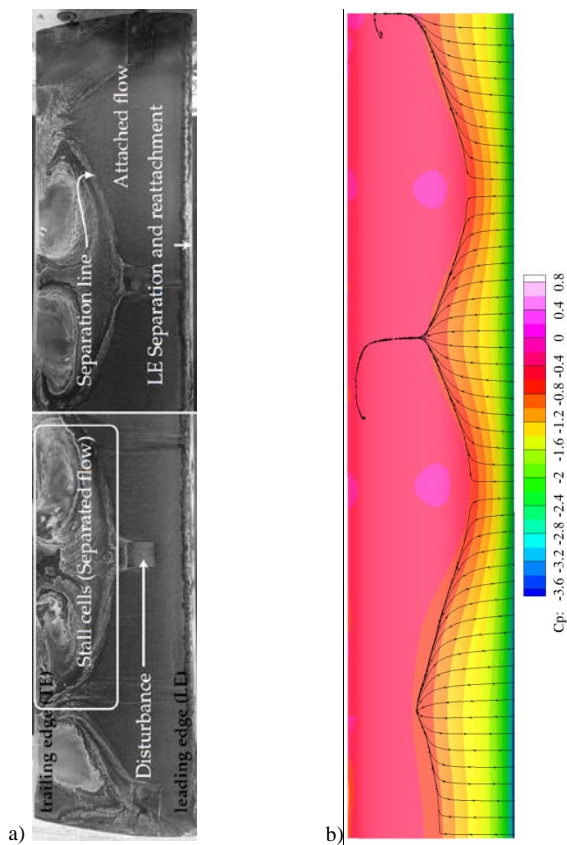
Figure 9. Generation of 3D mushroom structures on a S826 airfoil. a) Oil-flow visualisation, b) CFD reproduction of the 3D structures sing k-ω SST model.

airfoil polars and qualitatively predict the extent of stall cells. Further investigation of the numerical factors influencing the formation and magnitude of stall cells is currently being considered in order to arrive at more quantified comparisons.

Conclusions and future work

We presented an experimental investigation of the flow over an NREL S826 airfoil at three low Reynolds numbers (Re=40,000, 100,000 and 200,000) and have validated a series of SST RANS simulations at certain Reynolds numbers and angles of attack in terms of polars as well as formation of stall cells. From the measurements, clear 3D flow features in terms of both spanwise stall cells and corner flows were seen, especially at Reynolds numbers 100,000 and 200,000 and near stall angles of attack. It was seen that the CFD setup is able to accurately predict the

References

Ghassemi Isfahani, A., Webb, N. J., & Samimy, M. (2017). Stall Cell Formation over a Boeing Vertol VR-7 Airfoil. *55th AIAA Aerospace Sciences Meeting*, (January), 1–18. https://doi.org/10.2514/6.2017-1577

Manolesos, M., & Voutsinas, S. G. (2014). Geometrical characterization of stall cells on rectangular wings. *Wind Energy*, *17*(9), 1301–1314.

Michelsen, J. A. (1992). *Basis3D-a platform for development of multiblock PDE solvers*. Technical Note AFM92-05, Technical University of Denmark, Department of Fluid Mechanics.

Sarlak, H., Fr re, A., Mikkelsen, R., & Sørensen, J. N. (2018). Experimental investigation of static stall hysteresis and 3-Dimensional flow structures for an nrel S826 wing section of finite span. *Energies*, *11*(6). https://doi.org/10.3390/en11061418

Sarlak, H., Mikkelsen, R., Sarmast, S., & Sørensen, J. N. (2014). Aerodynamic behaviour of NREL S826 airfoil at Re=100,000. *Journal of Physics: Conference Series*, *524*, 012027. https://doi.org/10.1088/1742-6596/524/1/012027

Sørensen, N. N. (1995). *General purpose flow solver applied to flow over hills*. Technical University of Denmark, Ris{ø} National Laboratory for Sustainable Energy.

Winkelman, A. E., & Barlow, J. B. (1980). Flowfield model for a rectangular planform wing beyond stall. *AIAA Journal*, *18*(8), 1006–1008.